HHS Public Access

Author manuscript

J Neurovirol. Author manuscript; available in PMC 2019 February 01.

Published in final edited form as:

J Neurovirol. 2018 February ; 24(1): 62–74. doi:10.1007/s13365-017-0594-0.

Persistence of SIV in the brain of SIV-infected Chinese rhesus macaques with or without antiretroviral therapy

Stefanie Perez[1,‡], **Ann-Marie Johnson**[1], **Shi-hua Xiang**[2], **Jian Li**[3], **Brian T Foley**[4], **Lara Doyle-Meyers**[1], **Antonito Panganiban**[1,5], **Amitinder Kaur**[1,5], **Ronald S Veazey**[1,6], **Yuntao Wu**[7], and **Binhua Ling**[1,5]

[1]Tulane National Primate Research Center; Tulane University School of Medicine, Covington, Louisiana 70433, USA

[2]Nebraska Center for Virology, School of Veterinary Medicine and Biomedical Sciences, University of Nebraska, Lincoln, Nebraska, 68583, USA

[3]Department of Statistics, Tulane University School of Public Health and Tropic Medicine, New Orleans, Louisiana 70112, USA

[4]Theoretical Biology and Biophysics Group, Los Alamos National Laboratory, Los Alamos, New Mexico 87545, USA

[5]Department of Microbiology and Immunology, Tulane University School of Medicine, New Orleans, Louisiana 70112, USA

[6]Department of Pathology and Laboratory Medicine, Tulane University School of Medicine, New Orleans, Louisiana 70112, USA

[7]National Center for Biodefense and Infectious Diseases, Department of Molecular and Microbiology, George Mason University, Manassas VA 20110, USA

Abstract

Persistence of HIV-1 reservoirs in the central nervous system (CNS) is an obstacle to cure strategies. However, little is known about residual viral distribution, viral replication levels and genetic diversity in different brain regions of HIV-infected individuals on combination antiretroviral therapy (cART). Because myeloid cells particularly microglia are likely major reservoirs in the brain, and more microglia exist in white matter than gray matter in a human brain, we hypothesized the major viral reservoirs in the brain are the white matter reflected by higher levels of viral DNA. To address the issue, we used the Chinese rhesus macaque (ChRM) model of SIV infection, and treated 11 SIVmac251 infected animals including long-term nonprogressors with cART for up to 24 weeks. SIV reservoirs were assessed by SIV DNA levels in 16 specific regions of the brain and 4 regions of spinal cord. We found relatively high frequencies of SIV in basal ganglia and brain stem compared to other regions. cART-receiving animals had significantly

[*]Reprints or correspondence: Dr. Binhua Ling, Mailing address: Tulane National Primate Research Center, 18703 Three Rivers Road, Covington, LA 70433, Phone: (985) 871-6473, Fax: (985) 871-6509, bling@tulane.edu.

[‡]Current address: Hayward Genetics Center, Tulane University School of Medicine, New Orleans, Louisiana, 70112, USA

Conflict of interest

The authors declare no conflict of interest.

lower SIV DNA levels in the gray matter than white matter. Moreover, a shortened envelope gp120 with 21 nucleotide deletions and guanine-to-adenine hypermutations were observed. These results demonstrate that SIV enters the CNS in SIV-infected ChRM with a major reservoir in the white matter after cART, the SIV/ChRM/cART is an appropriate model for studying HIV CNS reservoirs and testing new eradication strategies. Further, examining multiple regions of the CNS may be needed when assessing whether an agent is successful in reducing the size of SIV reservoirs in the CNS.

Keywords

Human immunodeficiency virus; Simian immunodeficiency virus; rhesus macaque; central nervous system; reservoir; antiretroviral therapy

INTRODUCTION

The central nervous system (CNS) is one of the major anatomic HIV reservoirs in many HIV-infected patients, even those on highly suppressive combination antiretroviral therapy (cART), making it a major obstacle to HIV eradication and a cure. HIV reaches the CNS as early as 8 days post infection (Valcour *et al*, 2012). Although cART can effectively reduce HIV loads in cerebrospinal fluid (CSF), decreases are slower and delayed compared to viral loads in plasma. Further, despite low to absent levels in blood of patients on cART, residual viral RNA can often be detected in the brain, and serve as a persistent reservoir for viral replication, resulting in neuro-cognitive dysfunction, despite the absence of direct neuronal infection (Heaton *et al*, 2010). Intensification of cART does not seem to have an impact on this low-level viral production in the CNS (Eden *et al*, 2010). Currently, no drugs are capable of eradicating HIV reservoirs from the CNS.

Many aspects of the HIV/SIV reservoirs in the CNS are still unclear (Brew *et al*, 2015; Churchill and Nath, 2013). For instance, little is known regarding the cell types harboring persistent viruses, the distribution of virus and infected cells, viral diversity in tissues, or the possible genetic evolution in the brains of HIV-infected patients on cART. HIV diversity has been found in the brain of untreated patients showing neurological symptoms or opportunistic infections. Structural changes have also been observed in both the cerebral white and gray matter of HIV patients, even during suppressive cART in adults and adolescents (Fennema-Notestine *et al*, 2013). However, specifics of the distribution of HIV in white matter and gray matter are relatively unknown.

As different regions of the brain have different structure and function, the distribution and density of viral target cells is patchy, and the susceptibility of various regions of the brain to HIV infection differ. Few studies have extensively examined different regions of the CNS in HIV infection. A study of 6 brain tissues (meninges, frontal gray matter, frontal white matter, temporal subcortex, cerebellum and basal ganglia) of HIV-infected patients demonstrated that all patients had HIV DNA in the brain, but with variable levels (Zhao *et al*, 2009). However, most studies have only examined one or two regions of the brain, which may not accurately reflect the whole extent of cerebral HIV infection. The challenge of

studying multiple sections largely lies in the difficulties in accessing different, fresh brain tissues for sampling. To address these issues, animal models are essential.

Nonhuman primate (NHP) models have been instrumental in studying viral latency/persistence in the CNS (Clements *et al*, 2011) and continue to be used to address unanswered questions in the field (Garrido and Margolis, 2015). In SIV-infected, treatment-naïve macaques, SIV DNA can be detected throughout SIV infection, but RNA is usually only detectable at the later stages of SIV encephalitis (Williams *et al*, 2001). In pigtailed macaques (*Macaca nemestrina*) infected with neurovirulent viruses SIV/17E-Fr or SIV/DeltaB670, cART reduces viral replication and inflammation, but viral DNA is persistently detectable (Zink *et al*, 2010). Further, viral compartmentalization occurs between the meninges and the brain parenchyma, and virus in CSF more closely matches that of virus in the meninges at least in one animal infected with neuropathogenic isolates SIVsmH631Br and SIVsmE804E (Matsuda *et al*, 2013). However, the density of SIV infected cells can vary depending on the part of the brain sampled, which may confound interpretation of some studies, depending on what tissue sites and the number of sites biopsied (Brew *et al*, 2015). Thus far, it remains unclear as to whether cART can alter the distribution and density of SIV infection and addressing these issues is critical for new strategies targeting specific tissues for viral control and eradication.

Chinese rhesus macaques (ChRM) have been used in SIV pathogenesis and therapy studies, but rarely has the CNS been studied in this model. Recently, one study detected SIVmac239 RNA in the brain of SIV-infected ChRM resulting in neuropathological damage (Liu *et al*, 2016). In this study, we used SIVmac251, the most commonly used virus in the NHP SIV/AIDS model, as it more closely mimics the pathogenesis of HIV infection. Because myeloid cells such as perivascular macrophages and microglia are likely major reservoirs in the brain (Churchill *et al*, 2016; Dahl *et al*, 2014; Schnell *et al*, 2009; Williams *et al*, 2001), and because more microglia exist in white matter than gray matter in the human brain (Mittelbronn *et al*, 2001), we hypothesized that the white matter may be a more significant viral reservoirs in the brain than the gray matter which should be evident by higher DNA levels in the former. To address these issues, we examined SIV viral load in different regions of the CNS, compared viral distribution and genetic diversity in both SIVmac251-infected ChRM without cART and in animals on cART at the end of therapy. We also analyzed SIV gp120 envelope viral sequences isolated from the CNS. To our knowledge, this is the first time that SIV CNS reservoirs have been carefully examined in 20 regions of the CNS in a ChRM model, which closely mimics HIV infection and treatment in humans (Ling *et al*, 2010; Ling *et al*, 2014; Ling *et al*, 2013; Ling *et al*, 2007; Ling *et al*, 2002a; Ling *et al*, 2002b; Zhou *et al*, 2013).

RESULTS

Basic information of SIV-infected Chinese rhesus macaques with or without antiretroviral therapy

Eleven adult ChRM (4 male and 7 female) 7 to 22 years of age (mean age 13.9 ± 4.6 s.d.) were studied in the cART drug-treated (DTs) group. These animals were chronically SIVmac infected for 3 – 87.6 months prior to initiation of cART with relatively low plasma

viral loads (pVL). Animals received 3-drug antiretroviral therapy for varying periods of time ranging from 7 to 24 weeks. By the end of cART termination, all animals reached undetectable levels of pVL (limit of detection was 30 copies/ml) (Table 1). Another group of 12 animals (6 male and 6 female) 6.6 –14.5 years (mean age 10.2 ± 2.7 s.d.) were used for studies of plasma and CSF viral loads (cVL). These animals received cART for a short period of time (8 weeks) starting at 4 weeks post SIV infection, but they were off of cART for varying lengths of time when necropsied as shown in Table 2. All the viral loads on plasma and CSF shown were measured at the time of necropsy. No observable pathogenic lesions or evidence of SIV-associated encephalitis were detected by histologic examination.

CSF viral loads and their association with plasma viral loads in SIV-infected Chinese rhesus macaques

CSF viral load (cVL) levels were tested in 12 untreated animals. The levels ranged from undetectable (limitation of detection, 30 copies/ml) to 5.6 x 10^5 copies/ml. Compared to plasma viral loads, CSF had much lower levels (median 802 copies/ml, 25 – 75% percentile range: 30 – 63,275 copies/ml) than pVL (median 77,650 copies/ml, 25 – 75% percentile range: 366 – 282,750 copies/ml). However, cVL in untreated animals positively correlated with pVL levels (R=0.7686, p=0.0049) (Figure 1). In the cART group, cVL were not detectable because these animals had pVL at ~10^3 copies/ml or less even prior to initiation of cART. In addition, although the ages of cART group were relatively older than that of the untreated group, analysis did not show significant correlation between age and pVL in each group, therefore the impact of age discrepancy was considered insignificant in this study.

Frequency of positive SIV *env* DNA in different regions of the brain in animals with and without cART

To determine distribution and frequency of SIV infection in different regions of the brain and spinal cord in both untreated animals and DTs, we collected 16 brain regions that included corpus callosum, temporal lobe, frontal lobe, parietal lobe, occipital lobe etc. and 4 regions of the spinal cord. (Table 3). We used nested PCR to amplify SIV envelope gp120 from the 16 brain regions and spinal cord in 11 cART animals and 2 typical progressors which had sustained pVL at 10^4–10^6 copies/ml off treatment (Table 3). Detectable viral DNA was spread throughout many brain regions from different individuals on cART, although 6 of 11 cART animals (55%) had no virus detected in the CNS. The highest frequency of detectable SIV DNA in cART group was in basal ganglia (4 of 11, 36.4%) followed by brain stem (3 of 11, 27.3%). Because the regions of gray and white matter are not distinctly separated in midbrain, detection of SIV was not separated into gray and white matter in this region (Table 3). Not surprisingly, no SIV RNA was detected in any of the drug-treated animals.

SIV DNA levels were significantly reduced in gray matter but not in white matter in cART macaques compared to untreated animals

To assess viral distribution in the gray and white matters, we used real-time PCR and quantified SIV *gag* DNA levels in the 2 untreated TPs and 3 DTs that showed SIV positive signals in multiple regions of the brain. The detection limit of SIV *gag* DNA was 15 copies/10^6 cells. In DTs, virus DNA levels were significantly higher in white matter than in

gray matter ($p < 0.0001$) (Figure 2A); White matter had a median 455.7 copies/10^6 cells (25–75% percentile range: 221 – 773 copies/10^6 cells), whereas gray matter had a median 50 copies/10^6 cells (25–75% percentile range: 20 – 127.9 copies/10^6 cells). In contrast, gray matter had significantly higher viral levels than white matter in untreated SIV-infected animals ($p < 0.0001$) (Figure 2B); the former with a median 4184 copies/10^6 cells (25–75% percentile range: 1541 – 7697 copies/10^6 cells) and the latter with a median 472.5 copies/10^6 cells (25–75% percentile range: 205.6 – 1190 copies/10^6 cells). Viral levels were significantly higher in the untreated group than treated group in gray matter ($p < 0.0001$) (Figure 2C). However, strikingly, viral levels were not significantly different between the 2 groups in white matter, with median 567 copies/10^6 cells in untreated animals versus 530 copies/10^6 cells in treated animals ($p = 0.3494$) (Figure 2D).

Viral diversity and presence of extensive G-to-A hypermutations in brains of cART animals

Next, we assessed the degree of viral mutation and diversity in TPs and cART controllers. We studied 2 TPs and 2 of the 3 DTs (DT1 and DT2). Since the third animal (DT3) in DTs group had very low DNA levels (range of 10 to 10^3 copies/10^6 cells) that were barely measurable by SIV *gag* real-time PCR, PCR quantification of the long fragment of SIV envelope gp120 and sequencing was not obtained from this animal. The limitation of SIV *env* detection are similar to those of single genome analysis (SGA), which can only reliably be successful on plasma samples with viral loads above certain thresholds (~ 4000 copies/ml). Therefore, only those samples that had SIV DNA levels above 1x10^3 copies/10^6 cells in the 2 TPs and 2 DTs were analyzed. Overall, the sequences could be easily distinguished between individual animals. Each animal had its own clades of virus (Figure 3). The sequences from different regions of the brain in TP1 were highly homogeneous and close to the parental strain SIVmac251-PM series KC522165-KC522168 sequences (Del Prete *et al*, 2013) shown in Figure 3. The viral sequences from TP2 were a little more variable and close to KC522142, and the HM045 series (Yeh *et al*, 2010) with a significant 21 nucleotide deletion in the V4 region in most variants.

Sequences from cART animals DT1 and DT2 clustered closely, and were close to the SIVmac251 sequences of HQ187 series (Whitney *et al*, 2011) and the parental strain KC522142. Notably, DT2 had a high frequency of APOBEC3G (apolipoprotein B mRNA-editing, enzyme-catalytic, polypeptide-like 3G) hypermutations (G-to-A mutations), up to 75 (p value = 1.40E-11) in sequences derived from 2 regions: white matter of left parietal lobe and the brain stem (labeled as DT2-22L-W and DT2-24), when compared with sequences from other regions of the same animal and sequences from animal DT1 (Table 4).

Changes of the envelope gp120 of SIV in the CNS in untreated typical progressors and animals on cART

To determine if the mutations of nucleotides resulted in amino acid changes in envelope gp120 protein, we further analyzed the amino acid alignment. The sites with most changes were in the V1 and V4 loops. The V1 region was rich in serine (Ser or S) and threonine (Thr or T) especially in cART animals but these were not very glycosylated, which differs from HIV-1 M group that have more changes in glycosylation.

Sequences from different regions of the brain of TP2 showed some variations in the V1 and V4 regions. All but one of the TP2 variants had mutations from serine (Ser or S) to proline (Pro or P) at the V1-Loop position 155 (Figure 4). Further, the V4 loop had a 7 amino acid residue deletion at position 424 – 430 (QRPKERH) corresponding to a 21 nucleotide deletion in the majority of variants (Figure 4), similar to findings previously reported in virus found in peripheral blood in chronic but not acute phase of SIVmac251 infection (Yeh *et al*, 2010).

DISCUSSION

To our knowledge, this is the first study to evaluate viral reservoirs in up to 20 variant regions of the CNS in cART-treated SIV-infected ChRM model of HIV infection, although the SIV/ChRM model has been used to study SIV pathogenesis, as well as tissue reservoirs in lymphoid tissues and the gut (Ling *et al*, 2010; Ling *et al*, 2014; Ling *et al*, 2013; Ling *et al*, 2007; Ling *et al*, 2002a; Ling *et al*, 2002b; Marthas *et al*, 2001; Monceaux *et al*, 2007). As ChRM usually have lower viral loads and develop AIDS reletively slower than other SIV-susceptible nonhuman primates, it is not surprising that cVL were not detectable in SIV-infected LTNP of ChRM even prior to cART. However, undetectable cVL clearly did not mean that the virus did not enter the CNS of SIV-infected ChRM, as evidenced by the fact that SIV DNA could be detected in some of the LTNP even after cART. Similar to HIV-1 infected patients, cVL was positively correlated with pVL in typical progressors of ChRM without ART, indicating that ChRM with SIV infection mimics HIV-1 infection in the CNS.

In this study, we found that two sites, basal ganglia and brain stem, had the relatively highest frequencies of SIV detection in animals on ART from the 15 parts of the brain and spinal cord tested, indicating that these 2 sites might be major sites of viral persistence. However, it is possible that some of the viral DNA detected were from defective viruses. Our results are consistent with findings that despite the use of cART, cells carrying viral SIV DNA persist (Zink *et al*, 2010). In HIV-1 infected patients, abnormalities of the basal ganglia are associated with HIV dementia (Steinbrink *et al*, 2013). Although detection of viral DNA could not exclude defective virus, the results are still important because even isolated viral particles such as Tat can cause neurocognitive dysfunction, even in the absence of replication-competent virus. Determining which treated animals, or treated patients still have substantial CNS reservoir would be very important, as identification and characterization of cellular CNS reservoirs is a critical step to understand the mechanism of viral persistence in the CNS for the development of eradication strategies.

We found significant differences in SIV DNA viral loads between gray and white matter in the same group of animals in untreated as well as cART animals as shown in Figure 2. We also found that no significant differences in white matter viral loads between untreated and cART animals (Figure 2, D). Since the animals were not perfused when euthanized, it is possible that viruses examined in the gray matter could also contain vessel-associated blood-derived virus, as the human brain has higher blood flow in the gray matter than that of the white matter (Ballabh *et al*, 2004; Rengachary and Ellenbogen, 2005). However, the > 2 fold log10 disparity of SIV load between untreated and treated was unlikely due solely to virus

from blood contamination. The results suggested that antiretroviral therapy was effective in reducing viral DNA loads in the gray matter.

In contrast, the comparable viral levels in white matter between cART macaques and untreated group indicate that cART has little impact on this tissue, possibly due to poor penetration of antiretroviral drugs (Cory *et al*, 2013; Letendre *et al*, 2008)}. This result is in agreement with observations that HIV is more compartmentalized in the subcortical white matter in HIV-infected patients on cART (Nath, 2015). A number of studies have demonstrated that gray matter and/or white matter undergo significant structural alterations during HIV infection, even in patients receiving cART (Becker *et al*, 2012; Fennema-Notestine *et al*, 2013; Sarma *et al*, 2014; Wang *et al*, 2016). Although cellular reservoirs in the CNS are not fully understood, studies have suggested that cellular HIV or SIV reservoirs in the CNS likely include perivascular macrophages, long-lived microglia cells (Dahl *et al*, 2014; Schnell *et al*, 2009; Williams *et al*, 2001) and astrocytes (Churchill *et al*, 2009). Further, there are more microglia in white matter than gray matter in the human brain (Mittelbronn *et al*, 2001). Based on the brain regions we studied, the microglial populations harboring SIV in these two regions are the most likely major factors contributing to the differences in virus loads observed between gray and white matter.

While viral diversity and CNS compartmentalization (in CSF) have been identified in multiple studies (Sturdevant *et al*, 2012; Sturdevant *et al*, 2015), especially in HIV-1 infected patients with HIV-associated dementia (HAD) (Schnell *et al*, 2011) and during the early years after HIV transmission (Schnell *et al*, 2010), here we mainly focused on viral variants isolated from different specific regions of the brain. We found that each animal had its own clade of viruses, which agrees with the vast majority of other HIV and SIV data sets that suggest even if a person or animal is exposed to viral quasi-species from a donor, or from an experimental stock of SIV, primary infections in the recipient are almost always essentially clonal. TP1 appears to have a bottleneck effect that indicates a homogenous population was formed in the brain tissues both in white and gray matter. This is probably due to the brain blood barrier (BBB) selection effect, and that particular virus may have had the best fit in these brain tissues. Although TP2 showed relatively more diversification, dominant variants had a specific 21 nucleotide deletion in V4 region which was not found in parental virus stock, similar to findings from chronically SIVmac251 infected macaques, which the HM045 series sequences reported elsewhere (Yeh *et al*, 2010) and a 15 nucleotide deletion at the same region in sequences of U18019–U18021 series (Zhu *et al*, 1995), suggesting the mutated virus is likely emerging in chronic infection. Whether the mutation occurred after virus entered the brain or was derived from peripheral blood in chronic infection or whether the mutated virus is the source of blood mutated virus, remains to be determined, especially since other studies have demonstrated that meninges contain both CNS and peripheral blood-derived viruses (Matsuda *et al*, 2013) and there is a possibility of viral dissemination from the brain to the blood, or from the meninges to the brain parenchyma (Nath, 2015). Since the function of V4 loop is not well understood, it is unclear whether there is selective pressure on the variants to shorten the V4 loop by 7 residues (QRPKERH). However, further studies are needed to elucidate the virological and immunological significance of this shortening of the V4 loop.

Interestingly, sequences from white matter of the left parietal lobe and brain stem (22L-W and 24-W) in animal DT2 had high frequencies of G to A mutations (calculate *p* value, Table 2). These findings are in agreement with results in viral sequences isolated from brain (Depboylu *et al*, 2007) and semen of SIV-infected rhesus macaques (Whitney *et al*, 2011) as well as in HIV-1 infected patients receiving antiretroviral drugs (Knoepfel *et al*, 2011; Mullins *et al*, 2011), possibly because of APOBEC3G editing under the selective pressure of drug treatment. While most of these viruses could be defective, DNA genome like G-to-A mutated viruses have been detected in blood and rectal tissue (Fourati *et al*, 2012), and it is noteworthy that the G-to-A mutations were found only in the parietal lobe and brain stem, but no other sections of the brain in this animal, suggesting that viral hypermutation does not simultaneously occur in different sections of the brain.

Here we show that SIV-infected ChRM on cART are an excellent model to study neuro-AIDS and CNS reservoirs. Moreover, given that the virus enters the CNS as early as days after infection (Valcour *et al*, 2012), and pVL are comparable during acute infection between Indian rhesus macaques and ChRM even those become spontaneous LTNP (Ling *et al*, 2002a), we show that the CNS reservoir is established and persistent after SIV infection in both progressors and LTNP of ChRM. Of note, not all animals have detectable virus in the CNS, just like HIV-1 infected patients, many of whom also do not have detectable virus in brain tissues (Zhao *et al*, 2009). We also show that basal ganglia and brain stem may be the major sites of viral persistence in the CNS after antiretroviral therapy. Moreover, cART group had significantly reduced viral levels in gray matter but had no significant changes in viral levels in white matter when compared with untreated macaques. Finally, G to A hypermutations occurred in certain parts of the brain in a cART animal. Therefore, sampling multiple regions of the CNS may be necessary when assessing effects of novel approaches on reduction of the size of viral reservoirs in the CNS. Of note, we only used PMPA and FTC in this study, effect of more potent regimen of cART on CNS reservoir, such as the clinically recommended combination of tenofovir disoproxil fumarate (TDF)/emtricitabine (FTC)/dolutegravir (DTG), can be thoroughly tested in this unique nonhuman primate model of HIV infection.

MATERIALS AND METHODS

Ethics statement

Experimental procedures performed on rhesus macaques used in this study were approved by the Tulane Institutional Animal Care and Use Committee (IACUC). All animals were housed indoors throughout the study period at the Tulane National Primate Research Center (TNPRC). TNPRC facilities are fully accredited by the Association of Assessment and Accreditation of Laboratory Animal Care International (AAALAC) in accordance with standard husbandry practices following the Guide for the Care and Use of Laboratory Animals (NIH). To avoid unnecessary discomfort and pain to animals, anesthesia and analgesic medications were used appropriately under the direction of a veterinarian. Rhesus macaques were anesthetized with 10 mg/kg ketamine or 3 – 8 mg/kg telazol whenever they were removed from their home cage. For surgical procedures, animals were anesthetized with ketamine and maintained in a surgical plane of anesthesia using isoflurane. For physical

exams and blood sampling 10 mg/kg ketamine was used. Buprenorphine (0.01 mg/kg) or buprenorphine extended release (0.2 mg/kg) were the standard analgesics administered for painful procedures.

Animals and virus inoculation

Rhesus macaques (*Macaca mulatta*) of Chinese origin (ChRM) were used in this study. A total of 23 animals were studied, which included 11 out of 12 SIV-infected DTs with exclusion of the one that had detectable viral load at necropsy, and also included 12 chronically SIV-infected untreated animals for CSF and blood collection to monitor viral loads in plasma and cerebrospinal fluid (CSF). The 11 DTs were further studied from 15 brain regions described in details below in brain tissue collection. Two representative untreated animals were also studied from 15 brain regions for comparison. These 2 animals were typical progressors (TPs), which were infected for 1–3 years with a set point plasma viral loads at $10^4 \sim 10^6$ copies/ml. Basic animal information is shown in Table 1 for treated animals and Table 2 for untreated animals. Animals were intravaginally or intravenously infected with 500 $TCID_{50}$ SIVmac251. The stock SIVmac251 was obtained by culturing and harvesting from CEMx174 cells and provided by the Virus Characterization, Isolation, and Production Core of the TNPRC, and the sequences of the stock are available in GenBank (KC522165-168, KC522142) (Del Prete *et al*, 2013).

Antiretroviral therapy

During chronic SIV infection, 11 ChRM were treated with the reverse transcriptase inhibitors (R)-9-(2-phosphonylmethoxyypropyl) adenine (PMPA, tenofovir; 20 mg/kg), and beta-2′, 3′ dideoxy-3′-thia-5-fluorocytindine (FTC, emtricitabine; 40 mg/kg) daily by subcutaneous injection for 8– 24 weeks. Tenofovir and emtricitabine were generously provided by Gilead Sciences, Inc. (Foster City, CA) via Material Transfer Agreement.

Animal euthanasia and brain tissue collection

Animal euthanasia were consistent with the recommendations of the Panel on Euthanasia of the American Veterinary Medical Association. SIV-infected and/or drug-treated macaques were euthanized by first anesthetizing the animal with telazol and buprenorphine followed by a lethal i.v. injection of sodium pentobarbital following Tulane IACUC standards of operation (SOP). Tissues from brain and spinal cord (15 regions) were collected fresh and also snap frozen in liquid nitrogen during necropsies.

Quantification of viral RNA in plasma and cerebrospinal fluid in brain tissues

Plasma was separated from EDTA-treated whole blood by centrifugation at 700–800 × g for 10 min, conservatively remove plasma to avoid cell pellet, transferred to a second centrifuge tube and were centrifuged at 25,000xg for 1 hour to concentrate virus particles especially in samples from animals on cART with expected low viral loads. CSF was obtained from the dorsal cervical spine using TNPRC's standard operating procedures, CSF was centrifuged following the similar procedures as collection of plasma. SIV plasma viral loads (pVL) and CSF viral loads (cVL) were determined by real-time quantitative PCR analysis by the TNPRC Pathogen Detection and Quantification Core as described in detail elsewhere

(Monjure *et al*, 2014). High Pure Viral RNA kit (Roche, Indianapolis, IN, USA) was used for viral RNA extraction with minor modification. Primers and probe were designed from the conserved gag region covering detection of SIVmac239, SIVmac251 and SHIV viruses.

DNA extraction and quantification of viral DNA in brain tissues

Total genomic DNA was extracted from each tissue using a QIAamp DNA mini kit following the manufacturer's instructions. Determination of cell-associated SIV DNA viral loads for samples collected up to the time of necropsy followed methods for assays and analysis previously described elsewhere (Venneti *et al*, 2008). These standard methods have a 95% reliable threshold sensitivity of 30 total copies of SIV DNA or RNA per sample. Numbers of SIV copies were normalized to cell equivalents co-determined by quantitative PCR (qPCR) as described (Ling *et al*, 2014). For samples prepared from necropsy tissues, nested and qPCR/RT-PCR methods of analysis with reaction conditions and primer/probe sequences were performed as detailed in Hansen et. al (Hansen *et al*, 2011). DNA was prepared as above from multiple tissues to provide a greater amount of test material and a correspondingly lower limit of detection.

Viral DNA amplification by nested-PCR, sequencing and phylogenetic analysis

One to 0.5μg DNA was used for nested PCR to amplify SIV *envelope* gp120. The PCR products were purified using Clonetech PCR purification kit for population-based sequencing. Expand High Fidelity PCR (Taqman enzyme) was used to minimize PCR-induced sequence errors. The primers were as below: env-OF, 5′ CTATAATAGACATGGAGACACCCTTG, env-OR: 5′ CTTCTTGCACTGTAATAAATCCCTTCC; env-iF: 5′ GTAAAAAGTGTTGCTACCATTGCCAG, and env-iR: 5′ ACTGATACCCCTACCAAGTCATC. PCR reaction conditions included denaturation at 94°C for 2min, followed by 35 cycles of denaturation at 94°C for 50s, annealing at 55°C for 50s, and extension at 72°C for 2min, with an additional extension of 72°C for 7min. Two microliters of the first-round PCR products were used for nested PCR under the same thermocycling parameters. The PCR products were purified using high pure PCR product purification kit from Roche Life Science. SIV gp120 *env* sequences from newly isolated brain SIV variants were aligned with SIVmac239, and SIVmac251 reference sequences from the Los Alamos National Laboratory HIV Sequence Database and other relevant sequences from GenBank using the CLUSTAL X program (Thompson *et al*, 1997). The alignment was manually adjusted, and poorly aligned regions were excluded. All phylogenetic trees were constructed by PhyML program for a maximum likelihood tree starting with BioNJ neighbor-joining method, and the reproducibility of the branching orders was estimated by 1,000 bootstraps. Frequencies of G-to-A mutations were analyzed using the HIV Sequence Database Hypermut 2.0 program (http://hiv-web.lanl.gov). The amino acid sequences were aligned using Clustal W program of the BioEdit software. Highlighter for amino acid sequences v2.3.4 and analysis (Keele *et al*, 2008) were used to visualize the differences in amino acids between untreated and treated animals.

Statistical analysis

Non-parametric statistical analyses (Mann-Whitney test or Wilcoxon sign-rank test) were used to compare median viral loads in plasma and CSF, cell-associated SIV DNA in gray matter versus white matter, and untreated versus drug treated groups. The Spearman correlation was used to assess the relationship of levels of viral loads between plasma and CSF. GraphPad Prism 5.0 statistical software (GraphPad Software, Inc. San Diego, CA, USA) was used to analyze data and statistical results were set two-sided at $p < 0.05$ as significant.

Nucleotide sequence accession numbers

Viral *env* sequences were deposited in GenBank under accession numbers MF284715 – MF284792.

Acknowledgments

We thank M Duplantis, L Nieburg, Dr. P Didier and Dr. M Bouljihad of the Division of Comparative Pathology for tissue collection, and the animal care staff of the Division of Veterinary Medicine for their technical assistance.

This work was supported by NIAID R01 AI093307 (BL), NIMH R01 MH102144 (YW) and the TNPRC base grant OD011104. The funders had no role in study design, data collection and analysis, preparation of the manuscript or decision for publication.

Disclaimer: The content is solely the responsibility of the authors and does not necessarily represent the official views of the National Institutes of Health.

References

1. Ballabh P, Braun A, Nedergaard M. Anatomic analysis of blood vessels in germinal matrix, cerebral cortex, and white matter in developing infants. Pediatr Res. 2004; 56:117–24. [PubMed: 15128918]
2. Becker JT, Maruca V, Kingsley LA, Sanders JM, Alger JR, Barker PB, Goodkin K, Martin E, Miller EN, Ragin A, Sacktor N, Selnes O, Multicenter ACS. Factors affecting brain structure in men with HIV disease in the post-HAART era. Neuroradiology. 2012; 54:113–21. [PubMed: 21424708]
3. Brew BJ, Robertson K, Wright EJ, Churchill M, Crowe SM, Cysique LA, Deeks S, Garcia JV, Gelman B, Gray LR, Johnson T, Joseph J, Margolis DM, Mankowski JL, Spencer B. HIV eradication symposium: will the brain be left behind? J Neurovirol. 2015; 21:322–34. [PubMed: 25750070]
4. Churchill M, Nath A. Where does HIV hide? A focus on the central nervous system. Curr Opin HIV AIDS. 2013; 8:165–9. [PubMed: 23429501]
5. Churchill MJ, Deeks SG, Margolis DM, Siliciano RF, Swanstrom R. HIV reservoirs: what, where and how to target them. Nat Rev Microbiol. 2016; 14:55–60. [PubMed: 26616417]
6. Churchill MJ, Wesselingh SL, Cowley D, Pardo CA, McArthur JC, Brew BJ, Gorry PR. Extensive astrocyte infection is prominent in human immunodeficiency virus-associated dementia. Ann Neurol. 2009; 66:253–8. [PubMed: 19743454]
7. Clements JE, Gama L, Graham DR, Mankowski JL, Zink MC. A simian immunodeficiency virus macaque model of highly active antiretroviral treatment: viral latency in the periphery and the central nervous system. Curr Opin HIV AIDS. 2011; 6:37–42. [PubMed: 21242892]
8. Cory TJ, Schacker TW, Stevenson M, Fletcher CV. Overcoming pharmacologic sanctuaries. Curr Opin HIV AIDS. 2013
9. Dahl V, Gisslen M, Hagberg L, Peterson J, Shao W, Spudich S, Price RW, Palmer S. An example of genetically distinct HIV type 1 variants in cerebrospinal fluid and plasma during suppressive therapy. J Infect Dis. 2014; 209:1618–22. [PubMed: 24338353]

10. Del Prete GQ, Scarlotta M, Newman L, Reid C, Parodi LM, Roser JD, Oswald K, Marx PA, Miller CJ, Desrosiers RC, Barouch DH, Pal R, Piatak M Jr, Chertova E, Giavedoni LD, O'Connor DH, Lifson JD, Keele BF. Comparative characterization of transfection- and infection-derived simian immunodeficiency virus challenge stocks for in vivo nonhuman primate studies. J Virol. 2013; 87:4584–95. [PubMed: 23408608]

11. Depboylu C, Eiden LE, Weihe E. Increased APOBEC3G expression is associated with extensive G-to-A hypermutation in viral DNA in rhesus macaque brain during lentiviral infection. J Neuropathol Exp Neurol. 2007; 66:901–12. [PubMed: 17917584]

12. Eden A, Fuchs D, Hagberg L, Nilsson S, Spudich S, Svennerholm B, Price RW, Gisslen M. HIV-1 viral escape in cerebrospinal fluid of subjects on suppressive antiretroviral treatment. J Infect Dis. 2010; 202:1819–25. [PubMed: 21050119]

13. Fennema-Notestine C, Ellis RJ, Archibald SL, Jernigan TL, Letendre SL, Notestine RJ, Taylor MJ, Theilmann RJ, Julaton MD, Croteau DJ, Wolfson T, Heaton RK, Gamst AC, Franklin DR Jr, Clifford DB, Collier AC, Gelman BB, Marra C, McArthur JC, McCutchan JA, Morgello S, Simpson DM, Grant I, Group C. Increases in brain white matter abnormalities and subcortical gray matter are linked to CD4 recovery in HIV infection. J Neurovirol. 2013; 19:393–401. [PubMed: 23838849]

14. Fourati S, Lambert-Niclot S, Soulie C, Malet I, Valantin MA, Descours B, Ait-Arkoub Z, Mory B, Carcelain G, Katlama C, Calvez V, Marcelin AG. HIV-1 genome is often defective in PBMCs and rectal tissues after long-term HAART as a result of APOBEC3 editing and correlates with the size of reservoirs. J Antimicrob Chemother. 2012; 67:2323–6. [PubMed: 22687892]

15. Garrido C, Margolis DM. Translational challenges in targeting latent HIV infection and the CNS reservoir problem. J Neurovirol. 2015; 21:222–6. [PubMed: 25060298]

16. Hansen SG, Ford JC, Lewis MS, Ventura AB, Hughes CM, Coyne-Johnson L, Whizin N, Oswald K, Shoemaker R, Swanson T, Legasse AW, Chiuchiolo MJ, Parks CL, Axthelm MK, Nelson JA, Jarvis MA, Piatak M Jr, Lifson JD, Picker LJ. Profound early control of highly pathogenic SIV by an effector memory T-cell vaccine. Nature. 2011; 473:523–7. [PubMed: 21562493]

17. Heaton RK, Clifford DB, Franklin DR Jr, Woods SP, Ake C, Vaida F, Ellis RJ, Letendre SL, Marcotte TD, Atkinson JH, Rivera-Mindt M, Vigil OR, Taylor MJ, Collier AC, Marra CM, Gelman BB, McArthur JC, Morgello S, Simpson DM, McCutchan JA, Abramson I, Gamst A, Fennema-Notestine C, Jernigan TL, Wong J, Grant I. HIV-associated neurocognitive disorders persist in the era of potent antiretroviral therapy: CHARTER Study. Neurology. 2010; 75:2087–96. [PubMed: 21135382]

18. Keele BF, Giorgi EE, Salazar-Gonzalez JF, Decker JM, Pham KT, Salazar MG, Sun C, Grayson T, Wang S, Li H, Wei X, Jiang C, Kirchherr JL, Gao F, Anderson JA, Ping LH, Swanstrom R, Tomaras GD, Blattner WA, Goepfert PA, Kilby JM, Saag MS, Delwart EL, Busch MP, Cohen MS, Montefiori DC, Haynes BF, Gaschen B, Athreya GS, Lee HY, Wood N, Seoighe C, Perelson AS, Bhattacharya T, Korber BT, Hahn BH, Shaw GM. Identification and characterization of transmitted and early founder virus envelopes in primary HIV-1 infection. Proceedings of the National Academy of Sciences of the United States of America. 2008; 105:7552–7. [PubMed: 18490657]

19. Knoepfel SA, Di Giallonardo F, Daumer M, Thielen A, Metzner KJ. In-depth analysis of G-to-A hypermutation rate in HIV-1 env DNA induced by endogenous APOBEC3 proteins using massively parallel sequencing. Journal of virological methods. 2011; 171:329–38. [PubMed: 21111003]

20. Letendre S, Marquie-Beck J, Capparelli E, Best B, Clifford D, Collier AC, Gelman BB, McArthur JC, McCutchan JA, Morgello S, Simpson D, Grant I, Ellis RJ, Group C. Validation of the CNS Penetration-Effectiveness rank for quantifying antiretroviral penetration into the central nervous system. Arch Neurol. 2008; 65:65–70. [PubMed: 18195140]

21. Ling B, Mohan M, Lackner AA, Green LC, Marx PA, Doyle LA, Veazey RS. The large intestine as a major reservoir for simian immunodeficiency virus in macaques with long-term, nonprogressing infection. J Infect Dis. 2010; 202:1846–54. [PubMed: 21050120]

22. Ling B, Piatak M Jr, Rogers L, Johnson A-M, Russell-Lodrigue K, Hazuda DJ, Lifson JD, Veazey RS. Effects of Treatment with Suppressive Combination Antiretroviral Drug Therapy and the

Histone Deacetylase Inhibitor Suberoylanilide Hydroxamic Acid; (SAHA) on SIV-Infected Chinese Rhesus Macaques. PLoS ONE. 2014; 9:e102795. [PubMed: 25033210]

23. Ling B, Rogers L, Johnson AM, Piatak M, Lifson J, Veazey RS. Effect of combination antiretroviral therapy on Chinese rhesus macaques of simian immunodeficiency virus infection. AIDS research and human retroviruses. 2013; 29:1465–74. [PubMed: 23387294]
24. Ling B, Veazey RS, Hart M, Lackner AA, Kuroda M, Pahar B, Marx PA. Early restoration of mucosal CD4 memory CCR5 T cells in the gut of SIV-infected rhesus predicts long term non-progression. Aids. 2007; 21:2377–85. [PubMed: 18025874]
25. Ling B, Veazey RS, Luckay A, Penedo C, Xu K, Lifson JD, Marx PA. SIV(mac) pathogenesis in rhesus macaques of Chinese and Indian origin compared with primary HIV infections in humans. Aids. 2002a; 16:1489–96. [PubMed: 12131186]
26. Ling B, Veazey RS, Penedo C, Xu K, Lifson JD, Marx PA. Longitudinal follow up of SIVmac pathogenesis in rhesus macaques of Chinese origin: emergence of B cell lymphoma. J Med Primatol. 2002b; 31:154–63. [PubMed: 12390537]
27. Liu H, Xiao QH, Liu JB, Li JL, Zhou L, Xian QY, Wang Y, Zhang J, Wang X, Ho WZ, Zhuang K. SIV Infection Impairs the Central Nervous System in Chinese Rhesus Macaques. J Neuroimmune Pharmacol. 2016; 11:592–600. [PubMed: 27154032]
28. Marthas ML, Lu D, Penedo MC, Hendrickx AG, Miller CJ. Titration of an SIVmac251 stock by vaginal inoculation of Indian and Chinese origin rhesus macaques: transmission efficiency, viral loads, and antibody responses. AIDS Res Hum Retroviruses. 2001; 17:1455–66. [PubMed: 11679158]
29. Matsuda K, Brown CR, Foley B, Goeken R, Whitted S, Dang Q, Wu F, Plishka R, Buckler-White A, Hirsch VM. Laser capture microdissection assessment of virus compartmentalization in the central nervous systems of macaques infected with neurovirulent simian immunodeficiency virus. J Virol. 2013; 87:8896–908. [PubMed: 23720733]
30. Mittelbronn M, Dietz K, Schluesener HJ, Meyermann R. Local distribution of microglia in the normal adult human central nervous system differs by up to one order of magnitude. Acta Neuropathol. 2001; 101:249–55. [PubMed: 11307625]
31. Monceaux V, Viollet L, Petit F, Cumont MC, Kaufmann GR, Aubertin AM, Hurtrel B, Silvestri G, Estaquier J. CD4+ CCR5+ T-cell dynamics during simian immunodeficiency virus infection of Chinese rhesus macaques. J Virol. 2007; 81:13865–75. [PubMed: 17898067]
32. Monjure CJ, Tatum CD, Panganiban AT, Arainga M, Traina-Dorge V, Marx PA Jr, Didier ES. Optimization of PCR for quantification of simian immunodeficiency virus genomic RNA in plasma of rhesus macaques (Macaca mulatta) using armored RNA. J Med Primatol. 2014; 43:31–43. [PubMed: 24266615]
33. Mullins JI, Heath L, Hughes JP, Kicha J, Styrchak S, Wong KG, Rao U, Hansen A, Harris KS, Laurent JP, Li D, Simpson JH, Essigmann JM, Loeb LA, Parkins J. Mutation of HIV-1 genomes in a clinical population treated with the mutagenic nucleoside KP1461. PLoS One. 2011; 6:e15135. [PubMed: 21264288]
34. Nath A. Eradication of human immunodeficiency virus from brain reservoirs. J Neurovirol. 2015; 21:227–34. [PubMed: 25366659]
35. Rengachary, SS., Ellenbogen, RG. Principles of neurosurgery. 2. Elsevier Mosby; Edinburgh ; New York: 2005.
36. Sarma MK, Nagarajan R, Keller MA, Kumar R, Nielsen-Saines K, Michalik DE, Deville J, Church JA, Thomas MA. Regional brain gray and white matter changes in perinatally HIV-infected adolescents. Neuroimage Clin. 2014; 4:29–34. [PubMed: 24380059]
37. Schnell G, Joseph S, Spudich S, Price RW, Swanstrom R. HIV-1 replication in the central nervous system occurs in two distinct cell types. PLoS Pathog. 2011; 7:e1002286. [PubMed: 22007152]
38. Schnell G, Price RW, Swanstrom R, Spudich S. Compartmentalization and clonal amplification of HIV-1 variants in the cerebrospinal fluid during primary infection. J Virol. 2010; 84:2395–407. [PubMed: 20015984]
39. Schnell G, Spudich S, Harrington P, Price RW, Swanstrom R. Compartmentalized human immunodeficiency virus type 1 originates from long-lived cells in some subjects with HIV-1-associated dementia. PLoS Pathog. 2009; 5:e1000395. [PubMed: 19390619]

40. Steinbrink F, Evers S, Buerke B, Young P, Arendt G, Koutsilieri E, Reichelt D, Lohmann H, Husstedt IW. German Competence Network HA. Cognitive impairment in HIV infection is associated with MRI and CSF pattern of neurodegeneration. Eur J Neurol. 2013; 20:420–8. [PubMed: 23095123]
41. Sturdevant CB, Dow A, Jabara CB, Joseph SB, Schnell G, Takamune N, Mallewa M, Heyderman RS, Van Rie A, Swanstrom R. Central nervous system compartmentalization of HIV-1 subtype C variants early and late in infection in young children. PLoS Pathog. 2012; 8:e1003094. [PubMed: 23300446]
42. Sturdevant CB, Joseph SB, Schnell G, Price RW, Swanstrom R, Spudich S. Compartmentalized replication of R5 T cell-tropic HIV-1 in the central nervous system early in the course of infection. PLoS Pathog. 2015; 11:e1004720. [PubMed: 25811757]
43. Thompson JD, Gibson TJ, Plewniak F, Jeanmougin F, Higgins DG. The CLUSTAL_X windows interface: flexible strategies for multiple sequence alignment aided by quality analysis tools. Nucleic Acids Res. 1997; 25:4876–82. [PubMed: 9396791]
44. Valcour V, Chalermchai T, Sailasuta N, Marovich M, Lerdlum S, Suttichom D, Suwanwela NC, Jagodzinski L, Michael N, Spudich S, van Griensven F, de Souza M, Kim J, Ananworanich J, Group RSS. Central nervous system viral invasion and inflammation during acute HIV infection. J Infect Dis. 2012; 206:275–82. [PubMed: 22551810]
45. Venneti S, Bonneh-Barkay D, Lopresti BJ, Bissel SJ, Wang G, Mathis CA, Piatak M Jr, Lifson JD, Nyaundi JO, Murphey-Corb M, Wiley CA. Longitudinal in vivo positron emission tomography imaging of infected and activated brain macrophages in a macaque model of human immunodeficiency virus encephalitis correlates with central and peripheral markers of encephalitis and areas of synaptic degeneration. Am J Pathol. 2008; 172:1603–16. [PubMed: 18467697]
46. Wang B, Liu Z, Liu J, Tang Z, Li H, Tian J. Gray and white matter alterations in early HIV-infected patients: Combined voxel-based morphometry and tract-based spatial statistics. J Magn Reson Imaging. 2016; 43:1474–83. [PubMed: 26714822]
47. Whitney JB, Hraber PT, Luedemann C, Giorgi EE, Daniels MG, Bhattacharya T, Rao SS, Mascola JR, Nabel GJ, Korber BT, Letvin NL. Genital tract sequestration of SIV following acute infection. PLoS Pathog. 2011; 7:e1001293. [PubMed: 21379569]
48. Williams KC, Corey S, Westmoreland SV, Pauley D, Knight H, deBakker C, Alvarez X, Lackner AA. Perivascular macrophages are the primary cell type productively infected by simian immunodeficiency virus in the brains of macaques: implications for the neuropathogenesis of AIDS. J Exp Med. 2001; 193:905–15. [PubMed: 11304551]
49. Yeh WW, Rahman I, Hraber P, Coffey RT, Nevidomskyte D, Giri A, Asmal M, Miljkovic S, Daniels M, Whitney JB, Keele BF, Hahn BH, Korber BT, Shaw GM, Seaman MS, Letvin NL. Autologous neutralizing antibodies to the transmitted/founder viruses emerge late after simian immunodeficiency virus SIVmac251 infection of rhesus monkeys. J Virol. 2010; 84:6018–32. [PubMed: 20357097]
50. Zhao L, Galligan DC, Lamers SL, Yu S, Shagrun L, Salemi M, McGrath MS. High level HIV-1 DNA concentrations in brain tissues differentiate patients with post-HAART AIDS dementia complex or cardiovascular disease from those with AIDS. Sci China C Life Sci. 2009; 52:651–6. [PubMed: 19641870]
51. Zhou Y, Bao R, Haigwood NL, Persidsky Y, Ho WZ. SIV infection of rhesus macaques of Chinese origin: a suitable model for HIV infection in humans. Retrovirology. 2013; 10:89. [PubMed: 23947613]
52. Zhu GW, Liu ZQ, Joag SV, Pinson DM, Adany I, Narayan O, McClure HM, Stephens EB. Pathogenesis of lymphocyte-tropic and macrophage-tropic SIVmac infection in the brain. J Neurovirol. 1995; 1:78–91. [PubMed: 9222344]
53. Zink MC, Brice AK, Kelly KM, Queen SE, Gama L, Li M, Adams RJ, Bartizal C, Varrone J, Rabi SA, Graham DR, Tarwater PM, Mankowski JL, Clements JE. Simian immunodeficiency virus-infected macaques treated with highly active antiretroviral therapy have reduced central nervous system viral replication and inflammation but persistence of viral DNA. J Infect Dis. 2010; 202:161–70. [PubMed: 20497048]

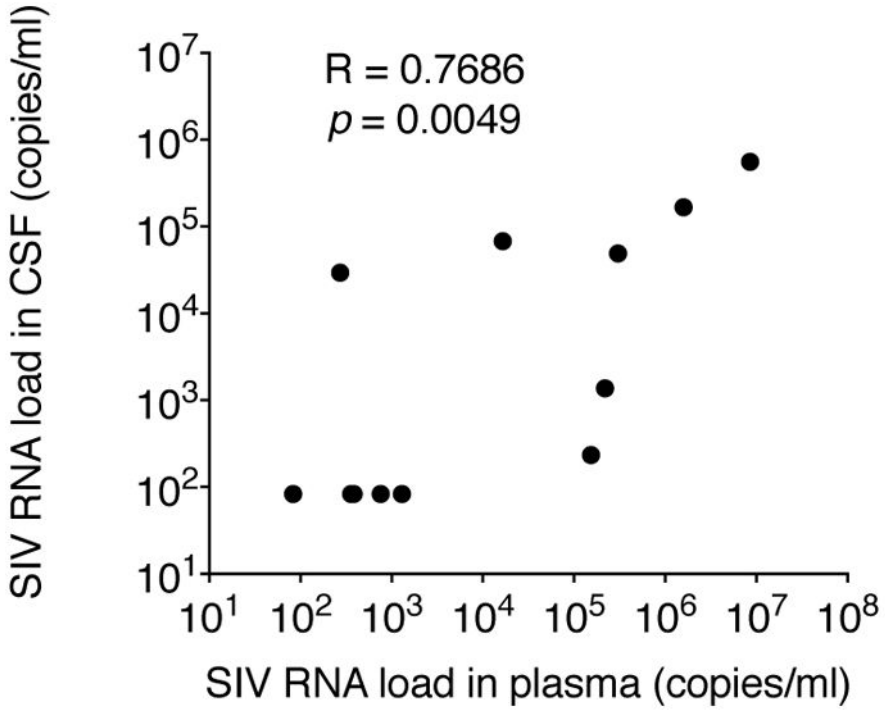

Figure 1.
Correlations between SIV RNA loads in plasma and cerebrospinal fluid (CSF) in untreated SIV-infected Chinese rhesus macaques.

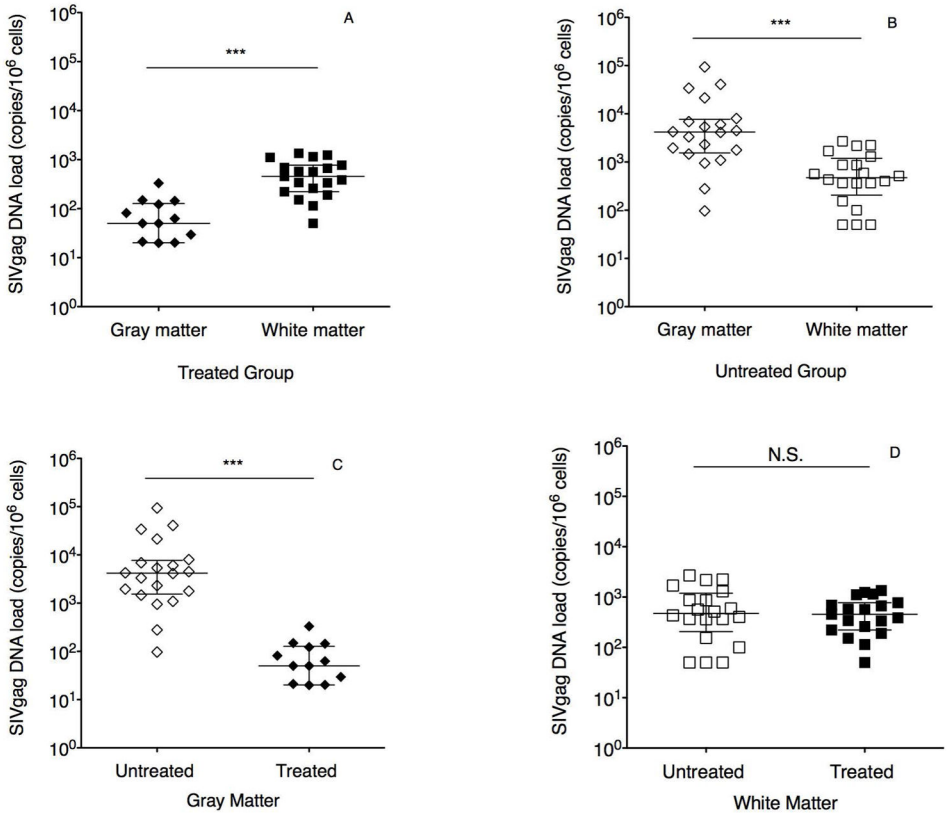

Figure 2.

Comparison of levels of SIV *gag* DNA between gray matter and white matter in the group of cART-treated (A) and untreated Chinese rhesus macaques (ChRM) (B), and levels of SIV *gag* DNA in gray matter between groups of untreated and cART-treated ChRM (C) and in white matter (D). Solid diamond, SIV *gag* DNA viral load in gray matter of ChRM on ART; solid square, SIV *gag* DNA viral load in white matter of ChRM on ART; Open diamond, SIV gag DNA viral load in gray matter of untreated ChRM; Open square, SIV *gag* DNA viral load in white matter of untreated ChRM; ***: $p < 0.0001$, N. S., no significance.

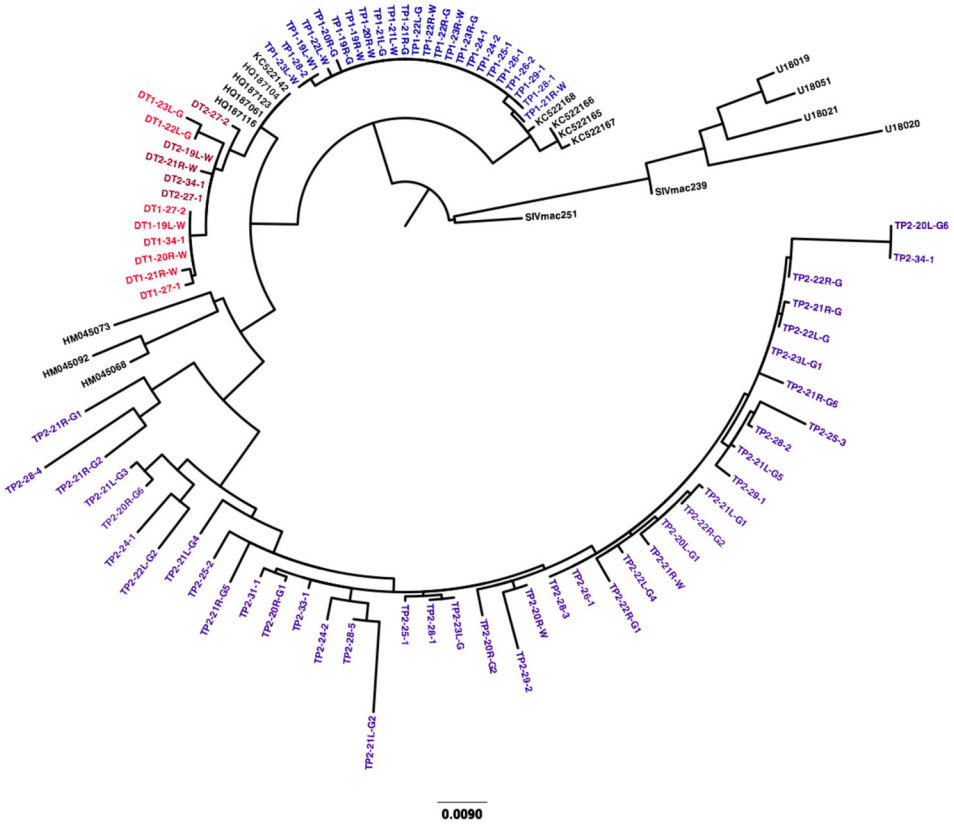

Figure 3.

Phylogenetic analysis of SIV envelope gp120 sequences of variants isolated from gray and white matter of different regions of the brain in 2 SIV-infected typical progressors without cART (TP1 and TP2) and 2 SIV-infected ChRM on cART (DT1 and DT2). Each sequence was named as animal name-label number of the brain followed with the left (L) or right (R)-gray or white with more than one sequence if followed with a number, for instance, TP2-20L-G1 (the 2nd typical progressor animal-left temporal lobe-gray matter sequence 1) represents sequence 1 that was isolated from the gray matter of left temporal lobe in the 2nd typical progressor animal. The tree scale bar indicates the number of substitutions per site.

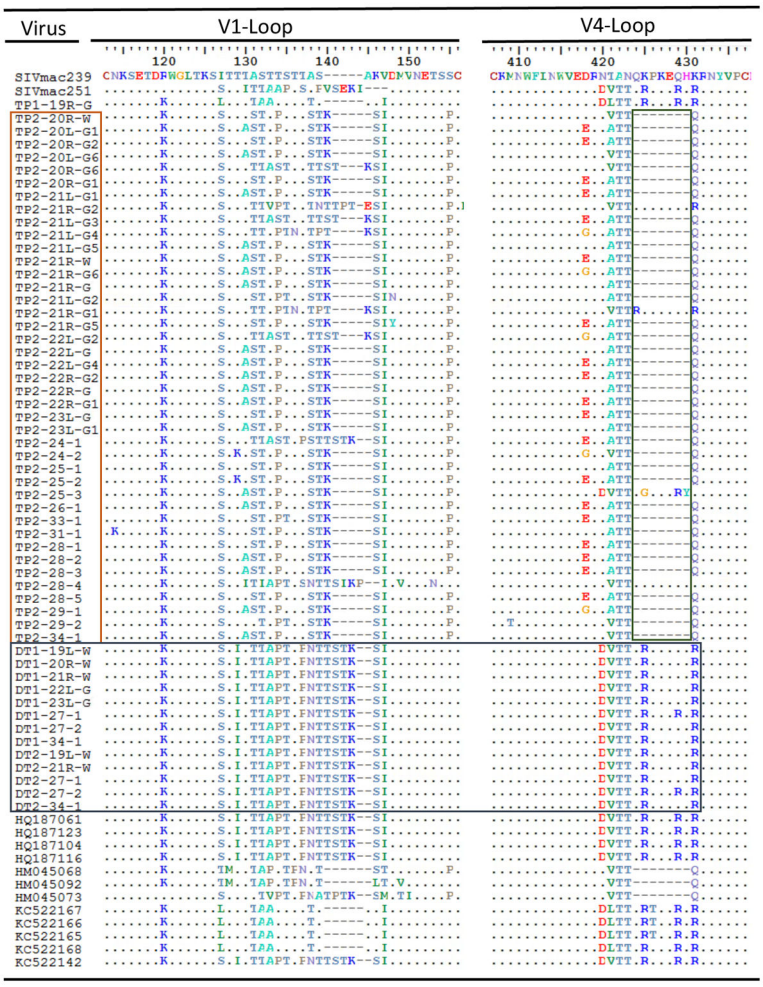

Figure 4.

Amino acid sequence comparison of SIV envelope V1 loop and V4 loop of SIVmac239, SIVmac251, variants from each sample group. TP1, test animal 1 (representative sequence); TP2, test animal 2; DT1, drug treated animal 1; DT2, drug treated animal 2. HQ series and HM series, GenBank sequences; and KC strains, parental strains. Dots represent amino acid identity with reference strain SIVmac239; dashes represent deletions.

Table 1

Basic information of SIV-infected Chinese rhesus macaques on antiretroviral therapy

Animal ID	Age	Sex	Length of infection pre-ART (month)	Route of infection	pVL pre- ART (copies/ml)	Period of ART (weeks)	pVL at the end of ART (copies/ml)	pVL after off ART (copies/ml)	cVL at the end of ART
CM61	12.9	M	16.8	I.V.	3.73E+04	24.0	UD	-	UD
DI98	11.7	M	16.8	I.V.	1.12E+03	8.0	UD	-	UD
DT93	21.7	F	36.0	I.V.	3.28E+03	10.0	UD	-	UD
EV57	16.6	F	3.0	I.V.	1.30E+05	8.0	UD	-	UD
FA10	15.4	F	36.0	I.V.	1.90E+02	24.0	UD	-	UD
FH20	8.8	M	16.8	I.V.	1.90E+02	24.0	UD	-	UD
GD41	7.4	M	3.0	I.V.	3.90E+05	8.0	UD	-	UD
GJ54*	13.9	F	32.4	I.V.	1.54E+03	8.0	UD	1.2E+03	UD
HG40	18.1	F	60.0	I.V.	2.87E+04	11.0	UD	-	UD
IV30	8.6	F	31.2	I.V.	4.65E+04	11.0	UD	-	UD
P015	20.0	F	87.6	I.V.	3.46E+02	7.0	UD	-	UD

*pVL rebound after 18 days of ART off

I.V.: intravenously; UD: undetectable

"-": unavailable, animals were on ART when euthanized

Table 2

Basic information of SIV-infected Chinese rhesus macaques

Animal ID	Age	Sex	Length of infection (month)	Route of infection	Plasma VL (copies/ml)	CSF VL (copies/ml)
BV71	14.5	F	17.9	I.V.	2.7E+02	3.0E+04
CC57	12.8	M	16.8	I.V.	8.5E+06	5.6E+05
CK24	12.4	F	16.9	I.V.	2.2E+05	1.4E+03
DI62	12.3	M	17.0	I.V.	1.5E+05	2.3E+02
DP02	11.7	F	17.8	I.V.	3.8E+02	UD
EM19	10.7	F	17.8	I.V.	1.3E+03	2.8E+01
EN60	10.3	M	17.2	I.V.	3.0E+05	4.9E+04
FJ69	9.3	M	16.6	I.V.	1.6E+06	1.7E+05
FR70	8.5	F	15.6	I.V.	3.6E+02	UD
HC58	6.6	M	16.7	I.V.	UD*	UD
HD94	6.6	M	16.7	I.V.	7.6E+02	UD
IF29	6.9	F	30.3	I.V.	1.7E+04	6.8E+04

I.V.: Intravenously; UD, undetectable

Table 3

Frequency of SIV *env* DNA detection in different regions of the CNS

		Typical Progressor (n=2)		Animals on ART (n=11)	
Label	**Brain Region**	**Gray Matter**	**White Matter**	**Gray Matter**	**White Matter**
19L	Corpus callosum-left	-	100%	-	9.1%
19R	Corpus callosum-right	-	100%	-	18.2%
20L	Temporal Lobe-left	50%	100%	0.0%	18.2%
20R	Temporal Lobe-right	100%	100%	0.0%	18.2%
21L	Frontal Lobe-left	100%	100%	0.0%	9.1%
21R	Frontal Lobe-right	100%	100%	9.1%	18.2%
22L	Parietal Lobe-left	100%	100%	9.1%	18.2%
22R	Parietal Lobe-right	100%	100%	0.0%	9.1%
23L	Occipital Lobe-left	50%	100%	9.1%	18.2%
23R	Occipital Lobe-right	100%	100%	18.2%	9.1%
24	Brain Stem	100%		27.3%	
25	Basal ganglia	100%		36.4%	
26	Thalamus	100%		9.1%	
27	Hypothalamus	100%		18.2%	
28	Hippocampus	100%		18.2%	
29	Cerebellum	100%		0.0%	
	Spinal Cord				
31	Cervical	50%		9.1%	
32	Thoracic	50%		0.0%	
33	Lumbar	50%		9.1%	
34	Sacral/ coccygeal	50%		18.2%	

Table 4

Significant hypermutation of G to A in parietal lobe and brain stem in DT2

Sequence:	Muts:(Match Sites)[1]	Controls: (Control Muts)[2]	Rate Ratio[3]	Fisher Exact *p*-value
DT1-19L-W	8	9	0.89	0.6902
DT1-20R-W	7	9	0.78	0.7786
DT1-21R-W	7	9	0.78	0.7786
DT1-22L-G	4	10	0.4	0.9739
DT1-23L-G	7	10	0.7	0.8404
DT1-27-1	8	9	0.89	0.6902
DT1-34-1	7	9	0.78	0.7786
DT2-19L-W	5	9	0.56	0.9150
DT2-21R-W	4	9	0.44	0.9571
DT2-22L-W	**75**	**21**	**3.62**	**1.40E-11**
DT2-24-1	**75**	**21**	**3.62**	**1.40E-11**
DT2-27-1	4	9	0.44	0.9571
DT2-34-1	4	9	0.44	0.9571

Note:

[1] mutations that match the pattern used in each run. The default pattern is to look for G followed by RD (R = purine = G or A; D = A, G or T) which is the pattern most often mutated by APOBEC3G;

[2] other mutations that are not in APOBEC sties;

[3] the ratio of Muts/Controls (colum1/colum2).